Scientific Research Publishing

Atmospheric and Climate Sciences, 2026, 16(2), 339-357
https://www.scirp.org/journal/acs
ISSN Online: 2160-0422
ISSN Print: 2160-0414

Spatial and Temporal Variability of Summer Precipitation Extremes in Ethiopia and Their Possible Mechanisms

Alemnhe Getu Anteneh[1,2], Xin Geng[1*], Mulualem Abera Waza[1,3]

[1]Collaborative Key Laboratory of Meteorological Disaster, Ministry of Education (KLME), Joint International Research Laboratory of Climate and Environmental of Meteorological Disasters (CIC-FEMD), University of Information Science and Technology, Nanjing, China
[2]Amhara Regional State (ARS), Bahir Dar, Ethiopia
[3]Ethiopian Meteorology Institute (EMI), Addis Ababa, Ethiopia
Email: *gengxin@nuist.edu.cn

How to cite this paper: Anteneh, A.G., Geng, X. and Waza, M.A. (2026) Spatial and Temporal Variability of Summer Precipitation Extremes in Ethiopia and Their Possible Mechanisms. *Atmospheric and Climate Sciences*, **16**, 339-357.
https://doi.org/10.4236/acs.2026.162018

Received: February 16, 2026
Accepted: March 16, 2026
Published: March 19, 2026

Abstract

Ethiopia is a country that is highly vulnerable to climate change and often faces extreme weather events, creating great challenges related to food security, water resources, and socio-economic development. This study investigates the spatial-temporal characteristics of extreme rainfall (>30 mm·day^{-1}) over Ethiopia during June-September (JJAS) from 1981 to 2022 and their possible mechanisms. It is found that the climatological extreme rainfall frequency exceeds 10 - 12 days·yr^{-1} in the Ethiopian highlands but falls below 1 day·yr^{-1} in lowland regions, highlighting the important role of orography and monsoon dynamics. Trend analysis shows a clear dipole pattern, with significant increases in the western and southwestern regions ($p = 0.001$) and decreases in northern and northeastern areas of Ethiopia ($p = 0.003$ to 0.036). EOF analysis reveals a major highland-wide uniform mode (EOF1; 23% of variance) and a secondary north-south dipole mode (EOF2; 9%), which both exhibit evident interannual-to-interdecadal variabilities. While the EOF1 is closely linked to ENSO with a significant negative correlation ($R = -0.42$), PC2 shows a prominent upward trend with large-scale warming. After removing this trend, the interannual variability of PC2 is significantly associated with the preceding FMAM North Atlantic Tripole (NAT; $R = 0.35$) and the concurrent JJAS Indian Ocean Dipole (IOD; $R = 0.30$). Further analyses show that La Niña events can enhance the Somali low-level jet, strengthening southwesterly wind anomalies that transport abundant moisture and favor the occurrence of precipitation extremes. In contrast, the NATI and IOD induce anticyclonic circulations over eastern and northeastern Africa, respectively. These atmospheric responses

lead to moisture convergence in southern Ethiopia and divergence in the north. This promotes precipitation extremes, primarily in the southern part of the country. Our results highlight the importance of incorporating the three basin-scale air-sea coupled modes into early warning and seasonal forecasting systems, thereby enhancing adaptation strategies and flood-risk management for precipitation extremes.

Keywords

JJAS Extreme Rainfall, Ethiopia, ENSO, Indian Ocean Dipole, North Atlantic Tripole, Teleconnections, Flood Risk

1. Introduction

Climate extremes exert a disproportionately higher impact on human and natural systems compared to mean climate conditions [1] [2]. In Ethiopia, recurring droughts and heavy rainfall events are serious threats to livelihoods, food security, and water resources. The country is highly exposed to hydro-climatic shocks: over 80% of the population depends on rain-fed agriculture, and more than 85% of national electricity generation comes from hydropower [3] [4]. As part of the climate-sensitive East African region, Ethiopia is particularly vulnerable due to strong climate variability and limited adaptive capacity [5] [6].

Ethiopia experiences three distinct rainfall seasons. The Kiremt Season (June-September, JJAS) is the most important rainfall season for rain-fed agriculture and hydropower, contributing 50% - 80% of annual rainfall. The Belg Season (February-May, FMAM) serves as the second rainy period, while the Bega season (October-January, ONDJ) is predominantly dry and cold across most of the country [7]-[11]. The rainfall seasonality is controlled mainly by the meridional movement of the Inter-Tropical Convergence Zone (ITCZ) and the development of the East African summer monsoon circulation, including Congo-basin westerly, southwesterly low-level flow, and the Somali low-level jet [12]-[14]. The region is influenced by complex topography and the interplay between regional and global oceanic-atmospheric systems, which together produce pronounced spatiotemporal rainfall variability.

Large-scale climate modes exert substantial influence on Ethiopian precipitation. The El Niño-Southern Oscillation (ENSO), Indian Ocean Dipole (IOD), and North Atlantic Oscillation (NAO) have all been implicated in modulating rainfall variability [8] [15] [16]. El Niño events are typically associated with suppressed JJAS rainfall, increasing drought risk and crop failure, while La Niña events often enhance JJAS rainfall and may trigger flooding in vulnerable areas [14] [15] [17] [18]. These anomalies also influence rainfall onset and cessation, as well as the frequency and duration of wet spells [10] [13]. Positive IOD phases enhance the moisture transport from the western Indian Ocean and increase JJAS rainfall, especially when they co-occur with La Niña conditions [19]-[21]. Furthermore, variability

in the NAO impacts Ethiopian rainfall through atmospheric connections that modulate subtropical westerlies and the meridional positioning of moisture convergence, thereby shaping the spatial distribution of rainfall anomalies [12] [16].

In recent decades, the severity of extreme rainfall in Ethiopia has intensified, with increases in both the frequency and magnitude of high-impact daily precipitation [6] [22]-[24]. Continued warming of sea surface temperatures (SST) is expected to amplify hydro-climatic extremes in the region further [25]-[27]. Previous studies have commonly employed threshold-based indices such as R20 mm and R25 mm to identify extreme rainfall events. These works, however, have largely focused on seasonal totals or general characteristics [6] [22] [23]. In contrast, the present study investigates the spatiotemporal variability of extreme rainfall days and systematically links them to key oceanic and atmospheric drivers using empirical orthogonal function (EOF) analysis. This approach offers a more precise understanding of the region's most susceptible to extreme rainfall and elucidates the underlying basin-wide climate mechanisms. The rest of the paper is organized as follows: Section 2 describes the data and methods, Section 3 presents the results and discussion, and Section 4 summarizes the main conclusions.

2. Data and Methods

2.1. Study Area

Ethiopia is centrally located in the Horn of Africa, spanning approximately 3˚N - 15˚N latitude and 33˚E - 48˚E longitude. It shares borders with Eritrea, Djibouti, Somalia, Sudan, South Sudan, and Kenya. Covering an area of about 1.1 million km^2, the country encompasses a diverse range of landscapes, from lowland plains in the east and southeast to the central and northern Ethiopian Highlands, which exceed 4000 meters above sea level and are dissected by the Great Rift Valley (**Figure 1(a)** and **Figure 1(b)**). This topographic heterogeneity gives rise to distinct climate zones stratified by elevation. Traditional classification delineates three altitudinal belts: Dega (highland, >2600 m, <16˚C), Woina-Dega (midland, 1500 - 2500 m, 16˚C - 29˚C), and Kolla (lowland, <1500 m, >29˚C). The highlands play a critical role in modulating rainfall and temperature regimes, rendering Ethiopia particularly susceptible to seasonal and inter-annual climate variability [28]-[30].

2.2. Data and Methodology

This study uses gridded rainfall, sea surface temperature (SST), climate indices, and atmospheric reanalysis datasets to investigate the spatiotemporal variability of extreme JJAS rainfall over Ethiopia. Daily precipitation is obtained from CHIRPS v2.0 at 0.05˚ spatial resolution, which combines satellite observations with gauge data and has been widely applied in Ethiopian rainfall studies [24] [31]-[33]. Monthly SST fields are taken from the Extended Reconstructed Sea Surface Temperature version 5 (ERSSTv5; 2˚ × 2˚ resolution) [34]. The Niño-3.4

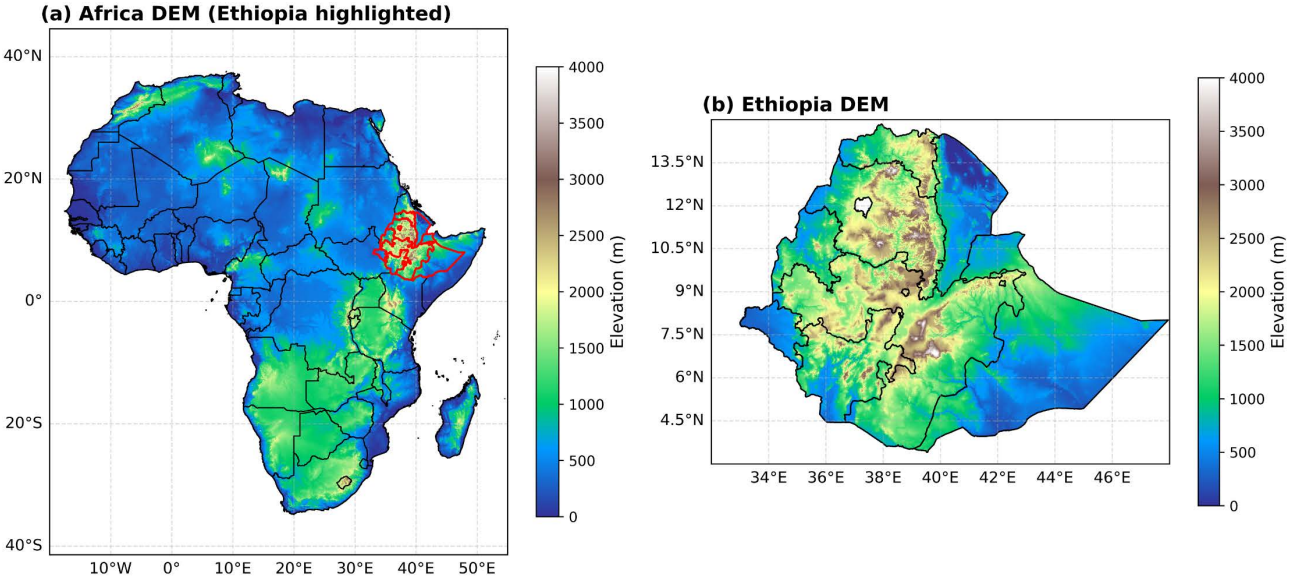

Figure 1. The locational and physical setting of Ethiopia. (a) Geographic position within Africa. (b) Topographic map showing major landforms, including the Highlands and Rift Valley. Elevation is indicated in meters (m) above sea level.

index is defined as the area-averaged SST anomalies over the Niño-3.4 region (5˚S - 5˚N, 120˚W - 170˚W), while the Indian Ocean Dipole (IOD) index is derived from the SST anomaly gradient between the western (50˚E - 70˚E, 10˚S - 10˚N) and southeastern (90˚E - 110˚E, 10˚S - 0˚) equatorial Indian Ocean. The North Atlantic Tripole Index (NATI) is calculated from SST anomalies over three distinct regions in the subpolar, subtropical, and tropical North Atlantic. Atmospheric circulation fields, including vertical and horizontal winds, specific humidity, and vertical velocity, are obtained from the NCEP/NCAR reanalysis dataset at 2.5˚ × 2.5˚ resolution [35] [36].

Studies have commonly employed threshold-based indices such as R20 mm and R25 mm to identify extreme rainfall events. These works, however, have largely focused on seasonal totals or general characteristics [6] [22] [23]. EOF analysis is applied to gridded annual JJAS extreme rainfall day counts (>30 mm) for 1981-2022. The data are linearly detrended at each grid point, cosine-latitude weighted, and grid cells with missing values near domain boundaries are masked. Mode significance is assessed using North's rule of thumb [37] [38]. Statistical significance is evaluated while accounting for serial correlation: correlations between EOF principal components and climate indices are tested using an effective sample size adjustment, and temporal trends are assessed using a trend-free prewhitened Mann–Kendall approach [39]. While the teleconnection influences are quantified using correlation and regression analyses [40] [41]. Composite and regression patterns are tested for statistical significance at the 95% confidence level using Student's t-test [42], and dominant rainfall periodicities are identified using wavelet power spectrum analysis [43] [44]. To test the robustness of this fixed threshold across Ethiopia's strong elevation and climate gradients, a sensitivity analysis was performed using a grid-cell-specific 95th percentile JJAS rainfall threshold. The

resulting spatial patterns and trends closely match those obtained with the fixed 30 mm day^{-1} threshold, indicating that the main conclusions are insensitive to the choice of extreme rainfall definition.

The North Atlantic Tripole (NAT) index (SSTA) is computed as the average of SSTA in regions A and C minus the SSTA in region B (**Figure 10(a)**), expressed as:

$$NATI = \left(\frac{SSTA\_a + SSTA\_c}{2} \right) - SSTA\_b \quad (1)$$

Where- region A (Subpolar North Atlantic) spans 45˚N to 60˚N and 57˚W to 10˚W, region B (Subtropical North Atlantic) covers 20˚N to 40˚N and 75˚W to 50˚W, and region C (Tropical North Atlantic) extends from 6˚S to 10˚N and 35˚W to 12˚W. To isolate internal variability from the forced warming signal, PC2 was linearly detrended prior to analysis. In addition, a multiple linear regression was applied to remove the influence of ENSO (Niño-3.4), the Indian Ocean Dipole (DMI), and the North Atlantic Tripole Index (NATI). The residual PC2 time series was then used for SST regression analysis.

3. Results and Discussion

3.1. JJAS Rainfall Climatology

The hydro-climatic heterogeneity in Ethiopia's territory, shown in **Figure 2**, exhibits contrasting climatic patterns between the moist highlands and arid lowlands during the JJAS rainy season. **Figure 2(a)** shows that the northwest, west, southwest, and central highlands of Ethiopia are the major hydrological storage during the JJAS rainy season, receiving total rainfall amounts of more than 800 - 1200 mm, characteristic of the core region of the Ethiopian summer monsoons under the influence of deep convection, high moisture transport, and orographic lift. During JJAS, seasonal rainfall amounts in the eastern and southeastern lowlands are much lower (<300 mm). **Figure 2(b)** differentiates these two areas by their seasonal rainfall contribution to the annual rainfall, whereby in the highland

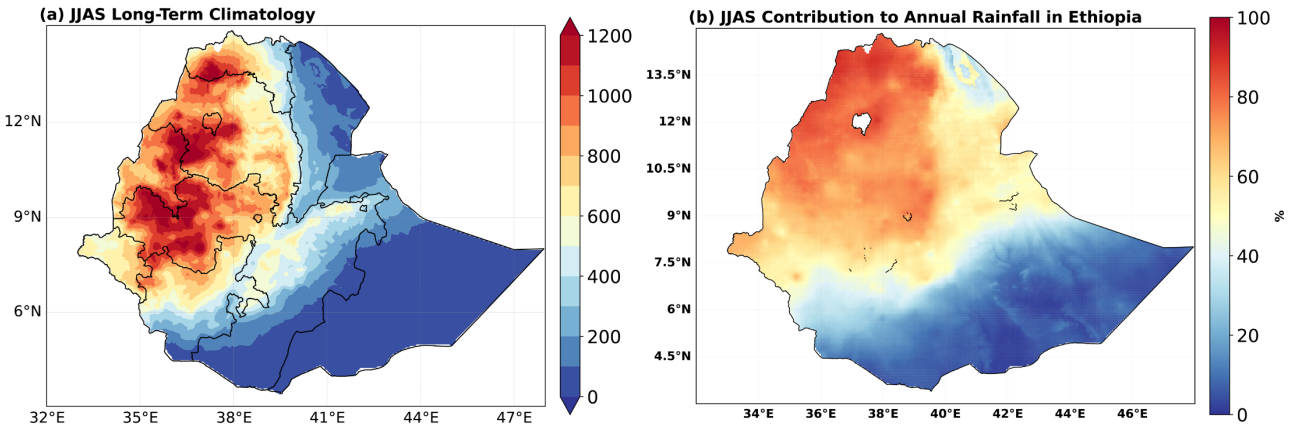

Figure 2. Spatial distribution of JJAS rainfall. (a) Long-term mean seasonal rainfall (mm). (b) Percentage contribution of JJAS rainfall to the annual total (%).

areas of northern and western Ethiopia, JJAS, or Kiremt, constitutes about (60% to over 80%) of the annual rainfall, characteristic of unimodal rainfall, which is largely influenced by the northward movements of the inter-tropical convergence zone (ITCZ). Conversely, the JJAS rainfall contributions in southern and southeastern zones are much lower than (20%), which are climatologically controlled by bimodal rainfall characteristics, with Belg (FMAM) and Bega (ONDJ) transitions defining the dominantly moist seasons, which are largely characterized by massive water supply from the transitions that fall during these seasons [10] [45].

3.2. Extreme Rainfall Climatology

Figure 3(a) shows the average climatology of the frequency of extreme rainfall days, and a strong and orderly spatial structure is apparent. The regions with the largest frequencies, above 11 days, are confined to the core area surrounding the northern, western, northeastern, central, eastern, southern, and southwestern Ethiopian highlands. There is a strong latitudinal decrease, with frequencies reducing to below 1.0 day per year in the southern, southeastern, and lowland parts of the domain, which is most likely associated with the topographic and associated meteorological controls on deep convection. In Figure 3(b), the inter-annual variability is shown, and a strong correspondence between the spatial distribution and the frequency is apparent. The regions of maximum frequency also display the maximum variability (Standard Deviation > 3.5), and indeed, the most extreme regions are the most variable, while the arid regions are both less frequent and less variable. This strong statistical equivalence between the spatial distribution of means and standard deviations demonstrates that the leading physical forcing mechanisms and associated controlling factors on the frequency also control the temporal instability.

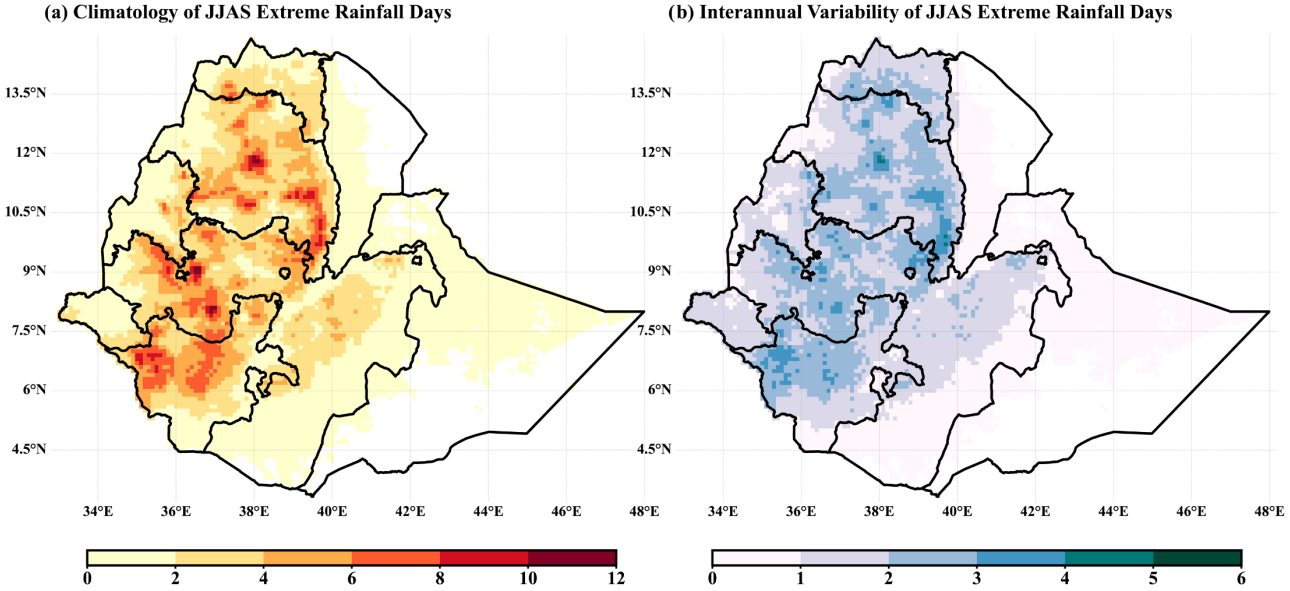

Figure 3. JJAS extreme rainfall characteristics, (a) Climatology of extreme rainfall events exceeding 30 mm/day (days/year). (b) Standard deviation of extreme events exceeding 30 mm/day (days).

3.3. Trend Analysis

Figure 4(a) presents the long-term trend pattern of JJAS extreme rainfall days over Ethiopia, which shows a high level of spatial heterogeneity with a clear northwest-southeast dipole. Significant increasing trends are found over the western and southwestern regions of the country, with isolated areas extending into the northern and eastern highlands. Conversely, significant decreasing trends are found over the northeastern part of the country, central Tigray, and the Southern Afar Zone 3. These results indicate that the changes are non-uniform at the regional level. Despite the significant trends at the local level, the country-averaged time series presented in Figure 4(b) shows a very weak and statistically insignificant increasing trend. This apparent stability reflects the cancellation of opposing regional trends. The time series further exhibits marked interannual variability, with seasonal extreme rainfall days ranging from approximately 3.0 to 6.5 days. The sub-regional averaged time series (Figure 4(c) & Figure 4(d)) reinforces this dipole structure. Central Tigray (Figure 4(c)) and Southern Afar

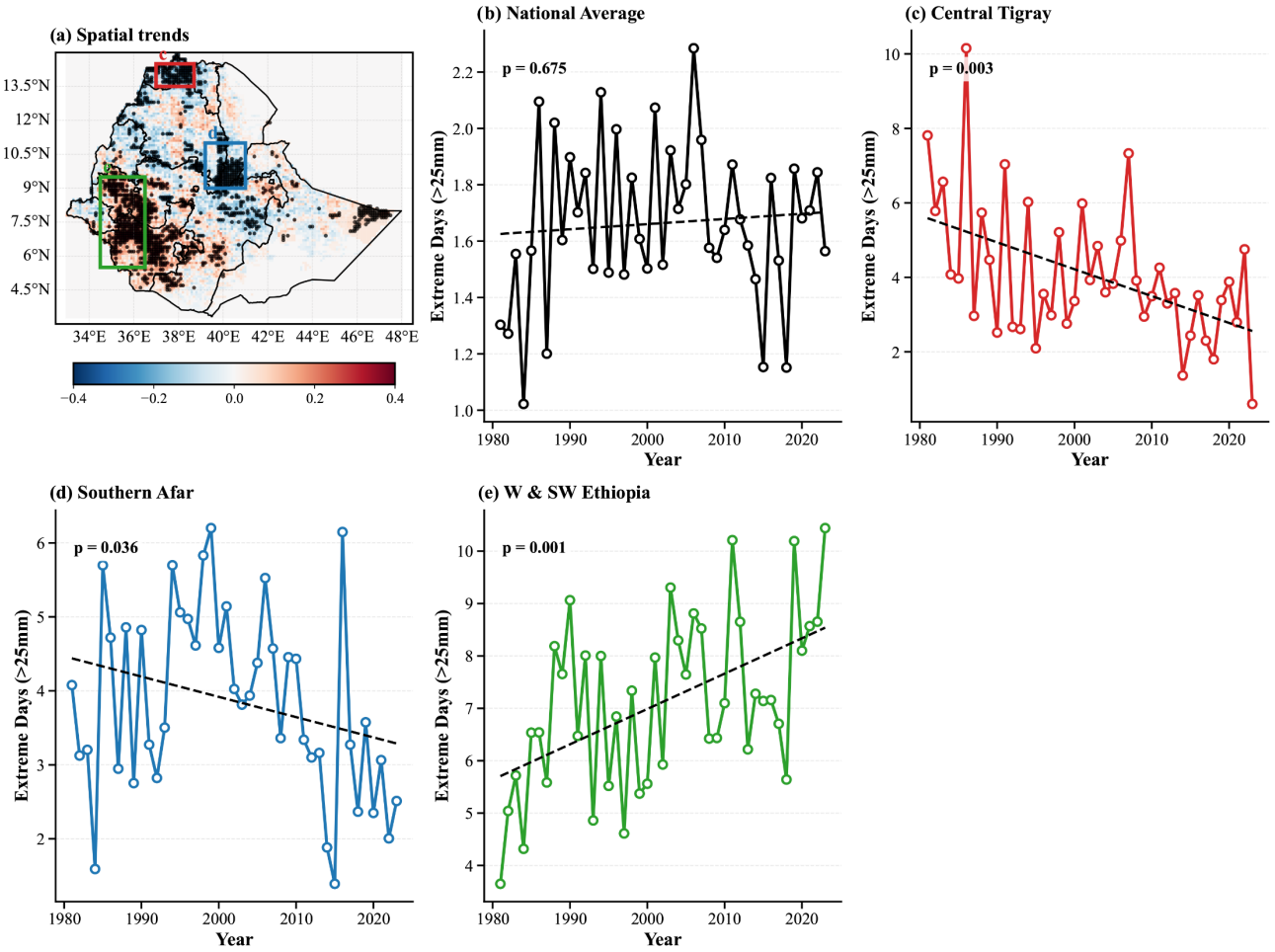

Figure 4. Trends and variability of JJAS extreme rainfall days (>30 mm·day^{-1}). (a) Spatial distribution of trends (days/year); stippling denotes significance at the 95% confidence level. (b) National areal-mean time series. (c)-(e) Regional time series for Central Tigray, Southern Afar (Zone 3), Western Ethiopia, and Southwestern Ethiopia, respectively.

Zone 3 (Figure 4(d)) experienced statistically significant declines in extreme rainfall days ($p = 0.003$, and $p = 0.036$, respectively). Conversely, (Figure 4(e)) western and southwestern Ethiopia exhibit significant increasing trends ($p = 0.001$). Taken collectively, these results show that Ethiopia is experiencing a significant reorganization of extreme rainfall. These findings are also supported by more recent studies, such as those by [22] [32], where a marked increasing trend in JJAS season rainfall was observed in some parts of Ethiopia.

3.4. Dominant Modes of JJAS Rainfall Extremes in Ethiopia

Figure 5 depicts the dominant modes of EOF and their associated Principal Component (PC) time series of extreme rainfall in the JJAS period over Ethiopia. The first EOF mode (EOF1) accounts for 23.1% of the total variance and is characterized by dominantly positive loadings over the central, southwestern, eastern, and northern Highlands. The spatial pattern reflects the combined influences of orographic effects and large-scale monsoon circulation systems. The corresponding PC time series exhibits strong variabilities at the 2-5-year band interannual cycles and at 10-18-year band quasi-decadal to decadal cycles in (Figure 6(a)). The second EOF pattern (EOF2) explains 9.2% of the variance and shows a clear north-south dipole configuration, with significant negative loadings in northeastern and

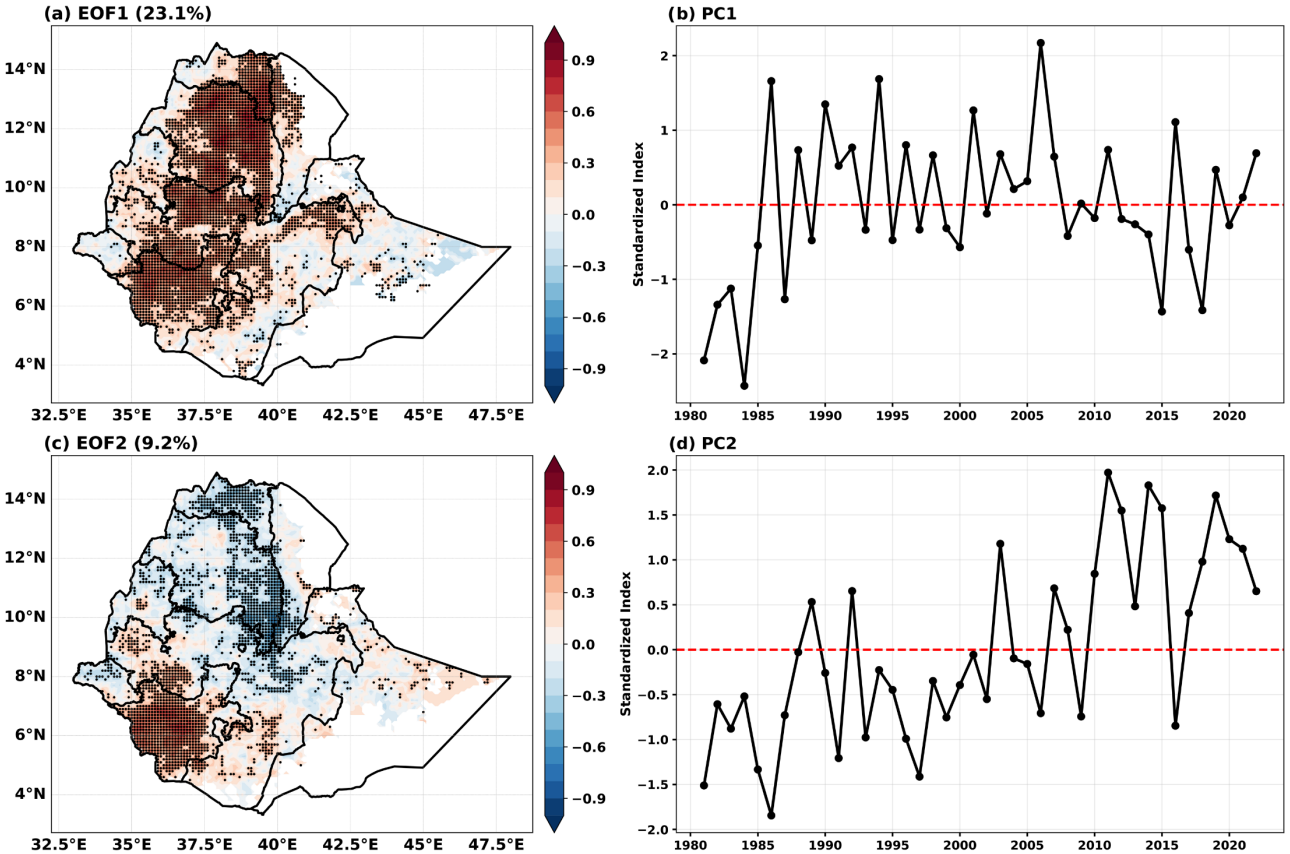

Figure 5. Dominant modes of JJAS extreme rainfall variability. (a) EOF1 and (c) EOF2 spatial variance patterns. (b) PC1 and (d) PC2 temporal scores. The variance explained (%) is indicated for each spatial mode.

central Ethiopia, while positive signals in the southwestern regions. This pattern reflects a consistent spatial distribution trend with Figure 4(a), and a clear inter-annual variability at the 3-6-year band and inter-decadal variability at the 8-12-year band in (Figure 6(b)). In general, these dominant modes demonstrate that JJAS extreme rainfall variability over Ethiopia is governed by a robust highland-centered signal, while secondary patterns capture spatial contrasts in rainfall extremes, underscoring the role of both orographic control and large-scale atmospheric dynamics in shaping flood-prone conditions across the country.

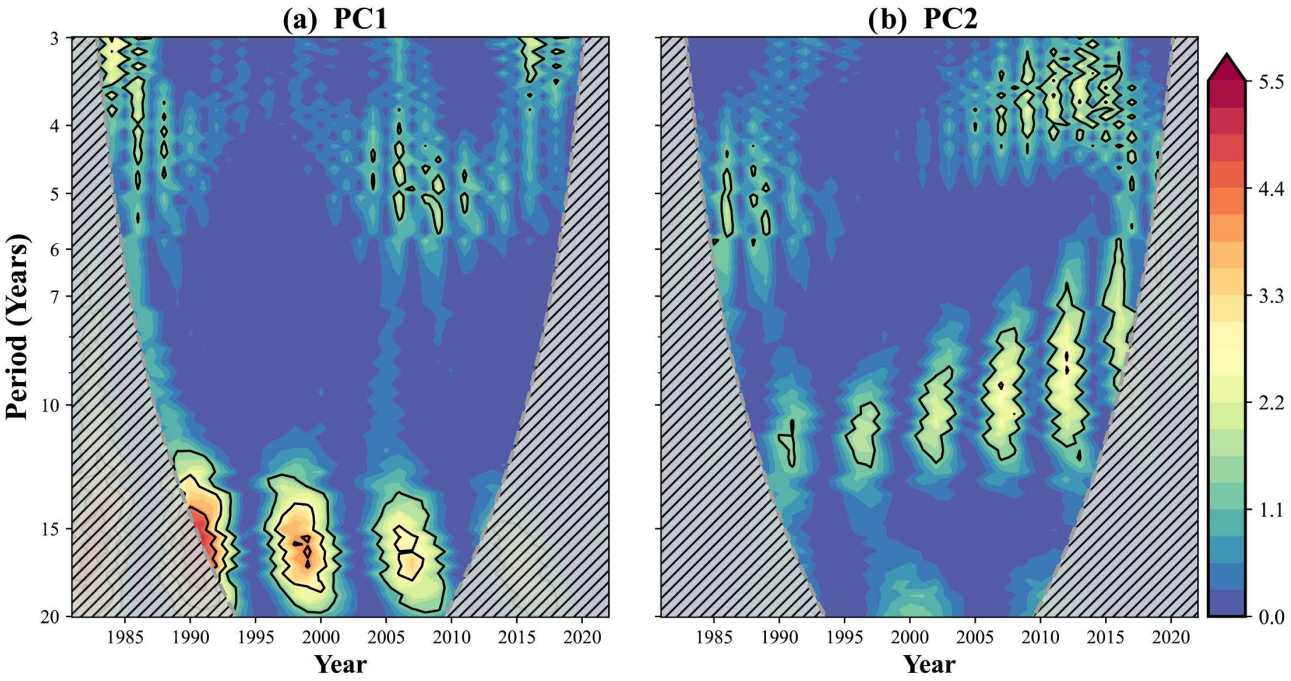

Figure 6. Continuous wavelet power spectra of JJAS extreme rainfall variability. (a) Power spectrum for PC1 and (b) for PC2. Color shading indicates wavelet power intensity; thick black contours denote the 95% significance level against a red noise background. The cross-hatched region identifies the cone of influence, where edge effects are significant.

3.5. Possible Mechanisms

Figures 7(a)-(h) displays the pattern evolution of the global SST anomalies from previous ONDJ to following ONDJ regressed on the first two PCs. PC1 is related to La Nina-like SST pattern during the previous winter (Figure 7(a)). Significant cold SST anomalies are found in the central and eastern equatorial Pacific and warm SST anomalies are detected in the western Pacific and Indian Oceans, suggesting that La Nina-like SST conditions enhance extreme rainfall in Ethiopia. Although the SST patterns in previous FMAM, simultaneous JJAS, and following ONDJ are generally consistent, the signal in the following ONDJ is weaker than that in the previous winter (Figure 7(c), Figure 7(e), and Figure 7(g)). This suggests that EOF1 may be mostly influenced by the ENSO events in previous winter. The PC2-regressed SST pattern displays a persistent global-scale warming signal throughout all four seasons, with cooling only occurring in the eastern Pacific and North Atlantic (Figure 7(b), Figure 7(d), Figure 7(f), and Figure 7(h)). This

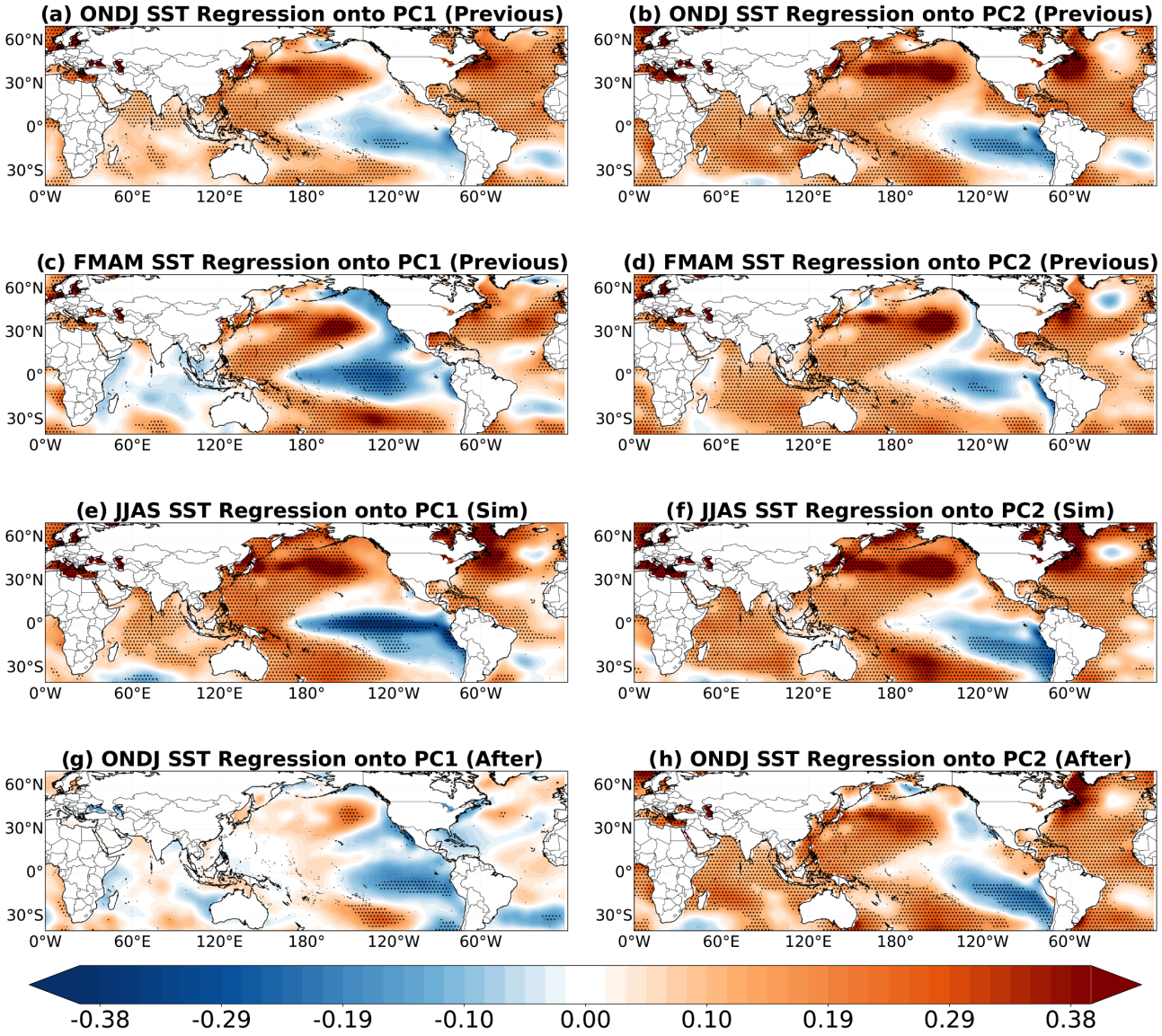

Figure 7. Regressions of (a), (b) previous ONDJ, (c), (d) previous FMAM, (e), (f) simultaneous JJAS, and (g), (h) following ONDJ global SST anomalies (˚C) onto JJAS PC1 and PC2. Shading shows regression coefficients, and stippling denotes the regressions are significant at the 95% confidence level.

pattern primarily resembles the global warming pattern [27] [46], suggesting that the PC2, especially the upward trend of PC2, may result from the global warming.

Figure 8 shows the relationship between the PC1 of Ethiopian JJAS extreme rainfall and the Niño 3.4 index during the previous ONDJ season. A significant negative correlation (R = −0.42) shows that La Niña conditions in boreal winter are strong indicators of increased JJAS rainfall and extreme events in Ethiopia. In contrast, El Niño phases tend to lead to reduced rainfall. The lead-lag correlation demonstrates the practical use of Niño 3.4 as a predictive indicator for early warning and flood risk preparedness in Ethiopia.

Next, we turn to investigate the possible mechanisms for the two EOF modes. Figure 9 illustrates the anomalous JJAS (700 hPa) low-level moisture-flux and its

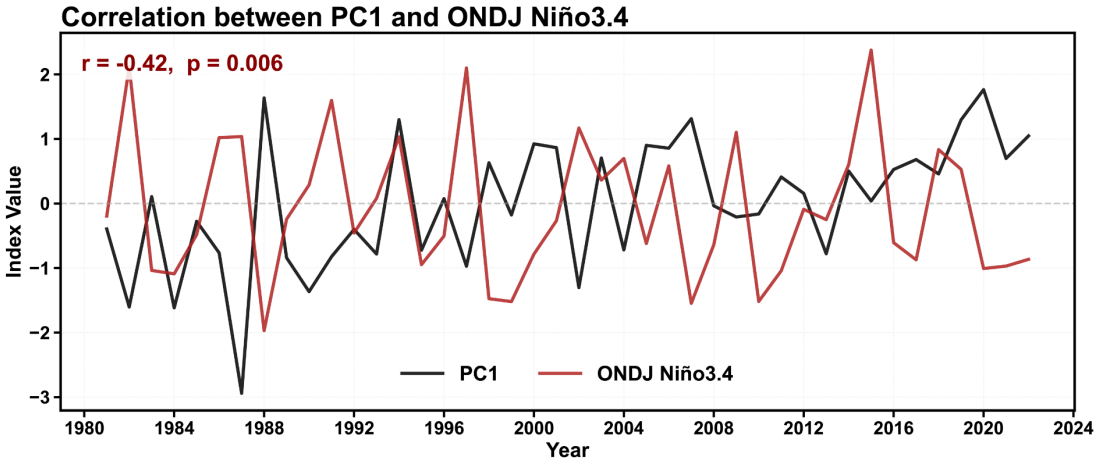

Figure 8. Standardized interannual relationship between the dominant principal component (PC1; black line) and the ONDJ Niño-3.4 Sea Surface Temperature index (red line). Both time series are standardized for the study period. Values in the legend represent the Pearson correlation coefficient (r) and the associated statistical significance (p-value).

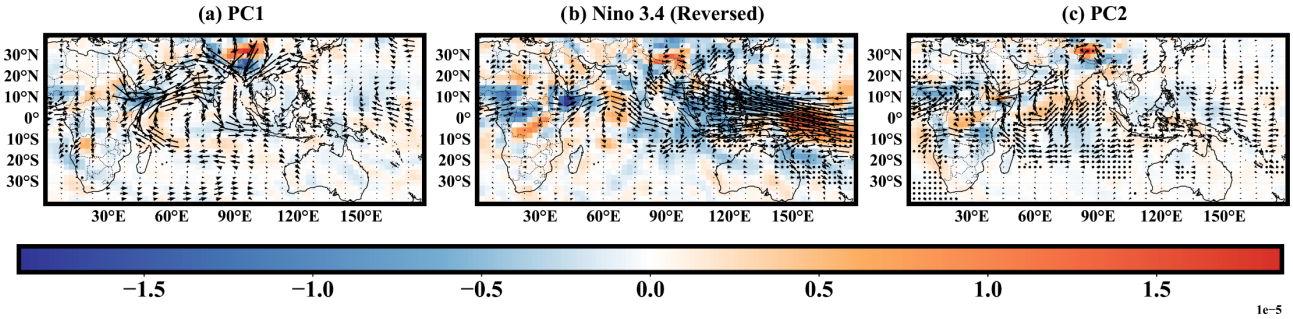

Figure 9. Regressions of JJAS 700hPa moisture flux (vectors; kg·m^{-1}·s^{-1}) and moisture-flux divergence (shading; 10^{-5} kg·m^{-2}·s^{-1}) onto (a) PC1, (b) reversed Niño-3.4, and (c) PC2. Blue shading indicates moisture convergence, while orange shading indicates moisture divergence. Black dots denote grid points significant at the 0.10 level.

divergence regressed onto the PC1, the reversed Niño-3.4 index, and the PC2. More highland-wide precipitation extremes correspond to a pronounced westerly and southwesterly moisture-flux corridor extending from the tropical Atlantic across the Congo Basin into the Ethiopian Highlands, where strong low-level moisture convergence is evident. This circulation is further reinforced by cross-equatorial southwesterly flow from the southwestern Indian Ocean via the Somali low-level jet, collectively providing the dominant moisture supply sustaining extreme JJAS rainfall over the central, western, and northwestern highlands. Figure 9(b) highlights the pattern related to La Niña-like SST forcing. In general, the pattern is largely similar to that related to PC1. La Niña can induce strengthened cross-equatorial flow and an enhanced Somali jet, promoting the convergence of Atlantic westerlies and Indian Ocean moisture over Ethiopia and establishing an efficient dual-ocean moisture conveyor belt. This configuration explains the strong relationship between La Niña episodes and rainfall/flood seasons that are above normal in JJAS. Figure 9(c) illustrates the anomalous moisture-flux related to PC2, where a clear dipole pattern with low-level divergence/dryness over northern Ethiopia and convergence/wetness over central and southern Ethiopia are evi-

dent. This is mainly driven by the anomalous easterly moisture flux from the western Indian Ocean sector that is possibly related to the global warming SST pattern.

Considering that PC2 also shows evident interannual-to-interdecadal variabilities, to determine the mechanisms of these components, we illustrate the regressed previous FMAM and simultaneous JJAS SST anomaly patterns onto the detrended PC2 in Figure 10. The regressed FMAM SST pattern is characterized by a distinct North Atlantic Tripole (NAT)-like structure**,** with significant warming over the subpolar North Atlantic, cooling over the mid-latitude western Atlantic, and weaker warming in the tropical Atlantic. However, the regressed simultaneous JJAS SST pattern displays a robust Indian Ocean Dipole (IOD)-like pattern, with pronounced warming in the western and central Indian Ocean and cooling over the eastern Indian Ocean and Maritime Continent. These results suggest that the North Atlantic SST forcing during FMAM and the IOD forcing during JJAS both have a significant influence on the variability of PC2.

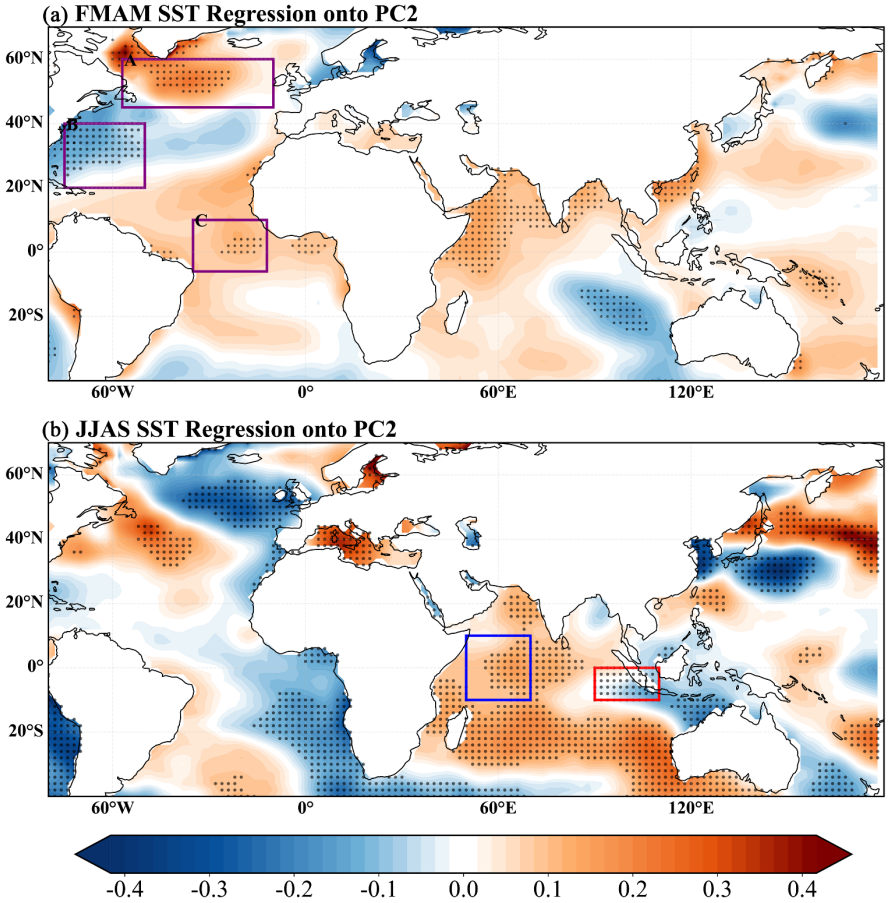

Figure 10. Regressions of (a) previous FMAM and (b) simultaneous JJAS global SST anomalies (˚C) onto JJAS PC2. Shading shows regression coefficients, highlighting the (a) North Atlantic Tripole (NATI) and (b) Indian Ocean Dipole (IOD) patterns. Black dots denote significance at the 0.10 level, and boxed regions indicate the index domains used in the analysis.

To further consolidate this argument, Figure 11 displays the time evolution of detrended PC2, FMAM NAT index, and JJAS IOD index. We find a close positive relationship between PC2 and the FMAM NAT index (R = 0.35), which is statistically significant at p = 0.024. This indicates that a positive phase of NAT can lead to a positive phase of EOF2, with more precipitation extremes in the south but less in the north. Figure 11(b) reveals a statistically significant positive relationship between PC2 and JJAS IOD index (R = 0.30), suggesting that a positive IOD favors more precipitation extremes in the southern but less in the northern part of Ethiopia. These results further confirm that the dipole mode of JJAS extreme rainfall over Ethiopia is strongly modulated by previous FMAM North Atlantic and concurrent Indian Ocean SST anomalies.

To further reveal the possible mechanisms, we show the regressed low-level moisture flux and its divergence onto the FMAM NAT index and JJAS IOD index in Figure 12. We can see that both positive NAT and IOD forcing are associated with strong cyclonic moisture flux anomalies over the western Indian Ocean and a prominent anticyclonic moisture flux anomalies over northeastern Africa. Correspondingly, we observe moisture convergence over southern Ethiopia but

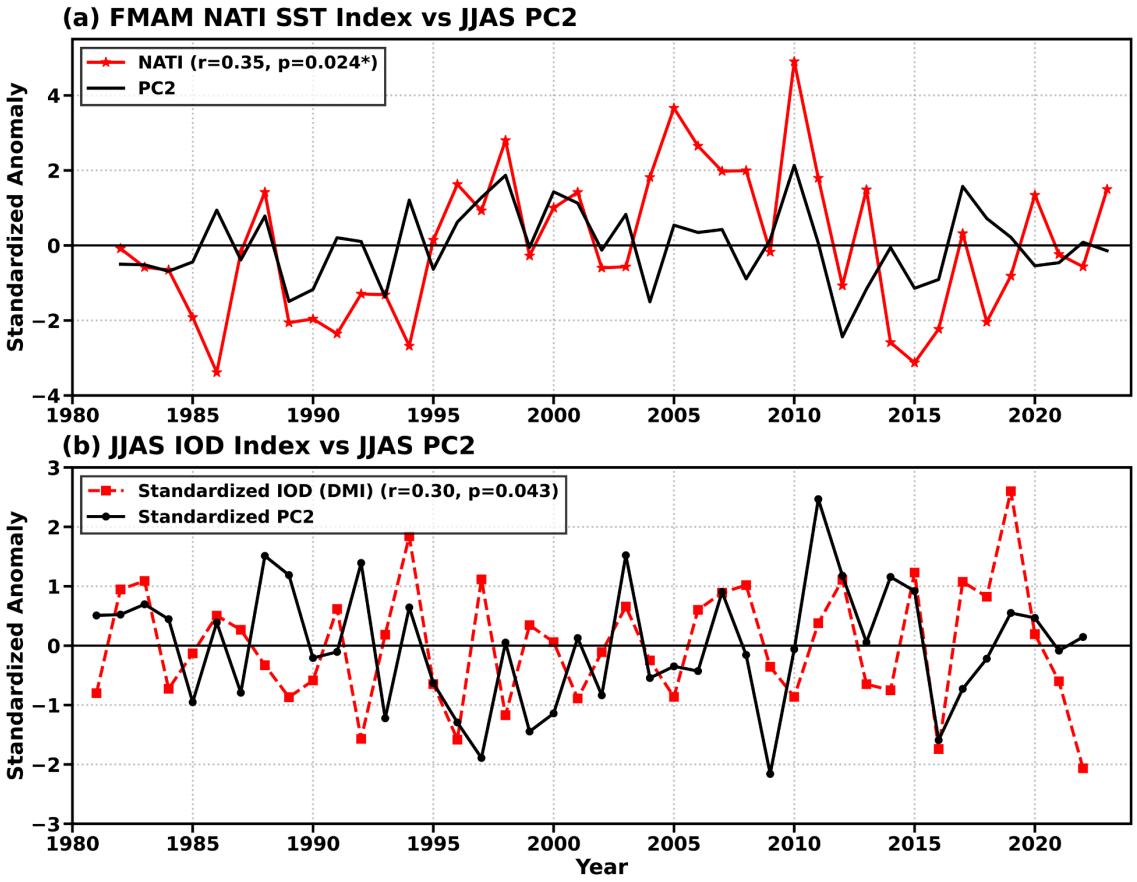

Figure 11. Interannual relationships between JJAS PC2 and regional climate indices. (a) Time series of JJAS PC2 (black) and previous FMAM North Atlantic Tripole Index (NATI; red). (b) Time series of JJAS PC2 (black) and simultaneous JJAS Indian Ocean Dipole (IOD/DMI; red). All series are standardized for the analysis period; correlation coefficients (r) and significance (p-values) are indicated.

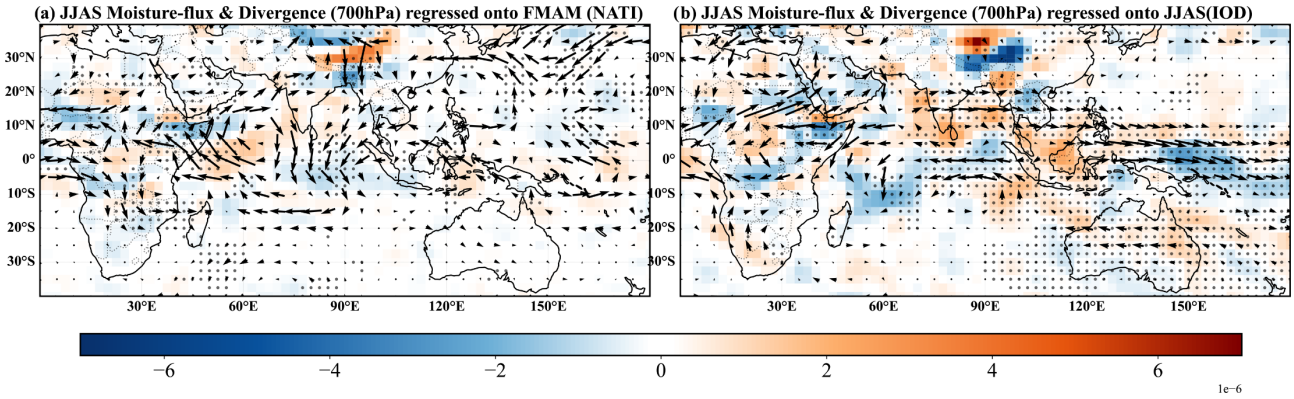

Figure 12. Regressions of JJAS 700 hPa moisture flux (vectors; kg·m^{-1}·s^{-1}) and moisture-flux divergence (shading; 10^{-6} kg·m^{-2}·s^{-1}) onto (a) preceding FMAM NATI and (b) simultaneous JJAS IOD. Shading represents regression coefficients, with blue (orange) indicating moisture convergence (divergence). Black dots denote regions significant at the 0.10 level.

moisture divergence over northern Ethiopia, which is well consistent with the positive phase of the EOF2 pattern.

4. Summary and Conclusion

Ethiopia is highly vulnerable to climate variability and extreme weather events, which create serious challenges to food security, water resources, and socio-economic development. This research utilized the high-resolution CHIRPS rainfall data to investigate the spatial and temporal variability and associated physical mechanisms of JJAS extreme rainfall days in Ethiopia from 1981 to 2022. The main conclusions are summarized as follows:

1) Climatologically, days with extreme rainfall are most frequent over the Ethiopian Highlands, with an annual frequency exceeding 10 to 12 days per year, compared to less than one day per year over the lowland regions.

2) The trends in extreme rainfall days over Ethiopia indicate a clear dipole pattern, with statistically significant increasing trends over western and southwestern regions ($p = 0.001$) and decreasing trends over northern and northeastern regions ($p = 0.003$ to 0.036).

3) EOF analysis indicates that extreme rainfall in the country shows a dominant highland-wide uniform mode (EOF1: 23% of total variance) and a secondary mode (EOF2: 9%) with a north-south dipole pattern.

4) EOF1 is found to be closely related to ENSO, as evidenced by a significant negative correlation between ONDJ Niño 3.4 and PC1 ($R \approx -0.42$). La Niña events tend to enhance the Somali low-level jet and the strength of southwesterly monsoon winds, which increase moisture convergence in the Ethiopian Highlands.

5) EOF2 shows a strong increasing trend related to global warming. Its interannual variability is related to the preceding FMAM NATI ($R \approx 0.35$) and concurrent JJAS IOD ($R \approx 0.30$). The NATI and IOD impact regional circulation patterns, resulting in a cyclonic anomaly in the western Indian Ocean and an anticyclonic anomaly in northeastern Africa. Moisture convergence is observed in southern Ethiopia, and divergence is observed in northern Ethiopia. The regional circula-

tion patterns enhance extreme rainfall in southern Ethiopia.

Overall, the study demonstrates that extreme rainfall in JJAS in Ethiopia is controlled by the combined influence of ENSO, NATI, and IOD. The study demonstrates the importance of ENSO, NATI, and IOD in early warning systems and seasonal forecasting. The study is important in developing a better understanding of extreme rainfall in Ethiopia.

Acknowledgements

First of all, I want to thank everyone who helped and encouraged me throughout this research. First and foremost, I would like to thank my supervisor, Prof. Xin Geng, for his insightful guidance, endless assistance, and inspiration during this research. Unrestricted conversations, helpful feedback, and gentle monitoring were essential to this study's success. Along with that, Mulualem Abera Waza has my deepest gratitude for his extraordinary kindness, inspiration, and continuous support throughout the study, and we were very grateful for his support and inspiration. Special thanks to Ato Arega Kebede, the esteemed President of the Amhara Regional State, whose humility, diligence, and dedication to education have been a source of inspiration. His moral and practical support was integral to my pursuit of higher education, particularly his instrumental role in enabling my master's studies in China. Finally, I would like to express my sincere gratitude to the Ministry of Commerce of the People's Republic of China (MOFCOM) for providing full scholarship support, which made this study possible. I also gratefully acknowledge Nanjing University of Information Science and Technology (NUIST) for offering excellent research facilities and a supportive academic environment that were essential for the successful completion of this work.

Author Contributions

Prof. Xin Geng: Conceptualization, Project administration, Resources, Supervision, Methodology, Investigation, Formal analysis, Validation, Visualization, Writing—original draft, Writing—review & editing.

Alemnhe Getu: Conceptualization, Methodology, Software, Data curation, Investigation, Formal analysis, Validation, Visualization, Writing—original draft, Writing—review & editing.

Mulualem Abera Waza: Conceptualization, Methodology, Software, Formal analysis, Visualization, Writing—review & editing.

Funding Information

This research received no specific grant from any funding agency in the public, commercial, or not-for-profit sectors.

Data Availability

CHIRPS precipitation data is available at
https://data.chc.ucsb.edu/products/CHIRPS-2.0/global_daily/netcdf/p05/

Monthly Sea Surface Temperature (SST) data were obtained from NOAA Physical Science Laboratory https://psl.noaa.gov/data/gridded/data.noaa.ersst.v5.html. For North Atlantic Tripole Index dataset extracted also from this source.

Nino3.4: https://psl.noaa.gov/data/correlation/nina34.data

IOD/DMI: https://psl.noaa.gov/data/timeseries/month/data/dmi.had.long.data

Atmospheric and Oceanic circulation variables with pressure level were obtained from IRI Columbia https://iridl.ldeo.columbia.edu/SOURCES/.NOAA/.NCEP-NCAR/.CDAS-1/.MONTHLY/.Intrinsic/.PressureLevel/

Conflicts of Interest

The authors declare no conflicts of interest regarding the publication of this paper.

References

[1] Peterson, T.C. and Manton, M.J. (2008) Monitoring Changes in Climate Extremes: A Tale of International Collaboration. *Bulletin of the American Meteorological Society*, **89**, 1266-1271. https://doi.org/10.1175/2008bams2501.1

[2] Tierney, J.E., Smerdon, J.E., Anchukaitis, K.J. and Seager, R. (2013) Multidecadal Variability in East African Hydroclimate Controlled by the Indian Ocean. *Nature*, **493**, 389-392. https://doi.org/10.1038/nature11785

[3] Teferi, E., Kassawmar, T., Bewket, W., Zeleke, G., Ayele, G.T., O'Donnell, G., *et al.* (2025) Rainfed Agriculture in Ethiopia: A Systematic Review of Green Water Management Pathways to Improve Water and Food Security. *Frontiers in Agronomy*, **7**, 1-18. https://doi.org/10.3389/fagro.2025.1418024

[4] FDRE-NAP (2019) Ethiopia's Climate Resilient Green Economy Strategy. National Adaptation Plan. Federal Democratic Republic of Ethiopia's National Adaptation Plan, 147.

[5] Pereira, L. (2017) Climate Change Impacts on Agriculture across Africa. Oxford Research Encyclopedia of Environmental Science.

[6] Gebrechorkos, S.H., Hülsmann, S. and Bernhofer, C. (2018) Changes in Temperature and Precipitation Extremes in Ethiopia, Kenya, and Tanzania. *International Journal of Climatology*, **39**, 18-30. https://doi.org/10.1002/joc.5777

[7] Gissila, T., Black, E., Grimes, D.I.F. and Slingo, J.M. (2004) Seasonal Forecasting of the Ethiopian Summer Rains. *International Journal of Climatology*, **24**, 1345-1358. https://doi.org/10.1002/joc.1078

[8] Segele, Z.T. and Lamb, P.J. (2005) Characterization and Variability of Kiremt Rainy Season over Ethiopia. *Meteorology and Atmospheric Physics*, **89**, 153-180. https://doi.org/10.1007/s00703-005-0127-x

[9] Korecha, D. and Sorteberg, A. (2013) Validation of Operational Seasonal Rainfall Forecast in Ethiopia. *Water Resources Research*, **49**, 7681-7697. https://doi.org/10.1002/2013wr013760

[10] Seleshi, Y. and Zanke, U. (2004) Recent Changes in Rainfall and Rainy Days in Ethiopia. *International Journal of Climatology*, **24**, 973-983. https://doi.org/10.1002/joc.1052

[11] Bekele-Biratu, E., Thiaw, W.M. and Korecha, D. (2018) Sub-Seasonal Variability of the Belg Rains in Ethiopia. *International Journal of Climatology*, **38**, 2940-2953. https://doi.org/10.1002/joc.5474

[12] Diro, G.T., Grimes, D.I.F. and Black, E. (2011) Large Scale Features Affecting Ethiopian Rainfall. In: Williams, C.J.R. and Kniveton, D.R., Eds., *African Climate and Climate Change*, Vol. 43, Springer, 13-50. https://doi.org/10.1007/978-90-481-3842-5_2

[13] Segele, Z.T., Lamb, P.J. and Leslie, L.M. (2009) Seasonal-to-Interannual Variability of Ethiopia/Horn of Africa Monsoon. Part I: Associations of Wavelet-Filtered Large-Scale Atmospheric Circulation and Global Sea Surface Temperature. *Journal of Climate*, **22**, 3396-3421. https://doi.org/10.1175/2008jcli2859.1

[14] Korecha, D. and Barnston, A.G. (2007) Predictability of June-September Rainfall in Ethiopia. *Monthly Weather Review*, **135**, 628-650. https://doi.org/10.1175/mwr3304.1

[15] Diro, G.T., Grimes, D.I.F. and Black, E. (2010) Teleconnections between Ethiopian Summer Rainfall and Sea Surface Temperature: Part I—Observation and Modelling. *Climate Dynamics*, **37**, 103-119. https://doi.org/10.1007/s00382-010-0837-8

[16] Degefu, M.A., Rowell, D.P. and Bewket, W. (2016) Teleconnections between Ethiopian Rainfall Variability and Global Ssts: Observations and Methods for Model Evaluation. *Meteorology and Atmospheric Physics*, **129**, 173-186. https://doi.org/10.1007/s00703-016-0466-9

[17] Camberlin, P. (1997) Rainfall Anomalies in the Source Region of the Nile and Their Connection with the Indian Summer Monsoon. *Journal of Climate*, **10**, 1380-1392. https://doi.org/10.1175/1520-0442(1997)010<1380:raitsr>2.0.co;2

[18] Mulualem Abera, W. and Wen, W. (2021) Interannual Variability of Seasonal Rainfall and Associated Circulations over Gambella, Ethiopia. *International Journal of Environmental Monitoring and Analysis*, **9**, 67-95. https://doi.org/10.11648/j.ijema.20210903.13

[19] Saji, N.H., Goswami, B.N., Vinayachandran, P.N. and Yamagata, T. (1999) A Dipole Mode in the Tropical Indian Ocean. *Nature*, **401**, 360-363. https://doi.org/10.1038/43854

[20] Manatsa, D., Matarira, C.H. and Mukwada, G. (2011) Relative Impacts of ENSO and Indian Ocean Dipole/Zonal Mode on East SADC Rainfall. *International Journal of Climatology*, **31**, 558-577. https://doi.org/10.1002/joc.2086

[21] Mwanthi, A.M. (2015) Investigating Linkages between the Subtropical Indian Ocean Dipole Mode and East Africa Rainfall during October-December. Master's Thesis, University of Nairobi, Nairobi. http://erepository.uonbi.ac.ke/handle/11295/91709

[22] Beyene, T.K., Jain, M.K., Yadav, B.K. and Agarwal, A. (2021) Multiscale Investigation of Precipitation Extremes over Ethiopia and Teleconnections to Large-Scale Climate Anomalies. *Stochastic Environmental Research and Risk Assessment*, **36**, 1503-1519. https://doi.org/10.1007/s00477-021-02120-y

[23] Teshome, A. and Zhang, J. (2019) Increase of Extreme Drought over Ethiopia under Climate Warming. *Advances in Meteorology*, **2019**, Article ID: 5235429. https://doi.org/10.1155/2019/5235429

[24] Waza, M.A., Zhu, W. and Teshome, A. (2025) Shifting Patterns of Ethiopian mam Rainfall: Effects of Sea Surface Temperature and Atmospheric Circulation (1981-2022). *International Journal of Climatology*, **45**, e8743. https://doi.org/10.1002/joc.8743

[25] Yan, X., Boyer, T., Trenberth, K., Karl, T.R., Xie, S., Nieves, V., *et al.* (2016) The Global Warming Hiatus: Slowdown or Redistribution? *Earth's Future*, **4**, 472-482.

https://doi.org/10.1002/2016ef000417

[26] Feyissa, G., Zeleke, G., Bewket, W. and Gebremariam, E. (2018) Downscaling of Future Temperature and Precipitation Extremes in Addis Ababa under Climate Change. *Climate*, **6**, Article No. 58. https://doi.org/10.3390/cli6030058

[27] IPCC (2023) Technical Summary. In: *Climate Change* 2023: *Synthesis Report. Contribution of Working Groups I, II and III to the Sixth Assessment Report of the Intergovernmental Panel on Climate Change*. Cambridge University Press. https://doi.org/10.1017/9781009157926.002

[28] Fazzini, M., Bisci, C. and Billi, P. (2015) The Climate of Ethiopia. In: Billi, P., Ed., *Landscapes and Landforms of Ethiopia*, Springer, 65-87. https://doi.org/10.1007/978-94-017-8026-1_3

[29] Extension, A. and Manual, T. (2022) Agroecology: An Extension Training Manual.

[30] Worku, T. and Tripathi, S.K. (2015) Watershed Management in Highlands of Ethiopia: A Review. *Open Access Library Journal*, **2**, e1481. https://doi.org/10.4236/oalib.1101481

[31] Funk, C., Peterson, P., Landsfeld, M., Pedreros, D., Verdin, J., Shukla, S., *et al.* (2015) The Climate Hazards Infrared Precipitation with Stations—A New Environmental Record for Monitoring Extremes. *Scientific Data*, **2**, Article ID: 150066. https://doi.org/10.1038/sdata.2015.66

[32] Gebrechorkos, S.H., Hülsmann, S. and Bernhofer, C. (2019) Long-Term Trends in Rainfall and Temperature Using High-Resolution Climate Datasets in East Africa. *Scientific Reports*, **9**, Article No. 11376. https://doi.org/10.1038/s41598-019-47933-8

[33] Dyer, E., Hirons, L. and Taye, M.T. (2022) July-September Rainfall in the Greater Horn of Africa: The Combined Influence of the Mascarene and South Atlantic Highs. *Climate Dynamics*, **59**, 3621-3641. https://doi.org/10.1007/s00382-022-06287-0

[34] Huang, B., Thorne, P.W., Banzon, V.F., Boyer, T., Chepurin, G., Lawrimore, J.H., *et al.* (2017) Extended Reconstructed Sea Surface Temperature, Version 5 (ERS-STv5): Upgrades, Validations, and Intercomparisons. *Journal of Climate*, **30**, 8179-8205. https://doi.org/10.1175/jcli-d-16-0836.1

[35] Kalnay, E., Kanamitsu, M., Kistler, R., Collins, W., Deaven, D., Gandin, L., *et al.* (1996) The NCEP/NCAR 40-Year Reanalysis Project. *Bulletin of the American Meteorological Society*, **77**, 437-471. https://doi.org/10.1175/1520-0477(1996)077<0437:tnyrp>2.0.co;2

[36] Kistler, R., Collins, W., Saha, S., White, G., Woollen, J., Kalnay, E., *et al.* (2001) The NCEP-NCAR 50-Year Reanalysis: Monthly Means CD-ROM and Documentation. *Bulletin of the American Meteorological Society*, **82**, 247-267. https://doi.org/10.1175/1520-0477(2001)082<0247:tnnyrm>2.3.co;2

[37] Hannachi, A., Jolliffe, I.T. and Stephenson, D.B. (2007) Empirical Orthogonal Functions and Related Techniques in Atmospheric Science: A Review. *International Journal of Climatology*, **27**, 1119-1152. https://doi.org/10.1002/joc.1499

[38] Hsu, C.J. and Zwiers, F. (2001) Climate Change in Recurrent Regimes and Modes of Northern Hemisphere Atmospheric Variability. *Journal of Geophysical Research: Atmospheres*, **106**, 20145-20159. https://doi.org/10.1029/2001jd900229

[39] Mondal, A., Kundu, S. and Mukhopadhyay, A. (2012) Rainfall Trend Analysis by Mann-Kendall Test: A Case Study of North-Eastern Part of Cuttack District, Orissa. *International Journal of Geology, Earth and Environmental Sciences*, **2**, 70-78.

[40] Wilks, D.S. (2011) Statistical Methods in the Atmospheric Sciences. Vol. 100, Academic Press.

[41] Montgomery, K.L., Vaughn, M.G., Thompson, S.J. and Howard, M.O. (2012) Heterogeneity in Drug Abuse Among Juvenile Offenders: Is Mixture Regression More Informative than Standard Regression? *International Journal of Offender Therapy and Comparative Criminology*, **57**, 1326-1346. https://doi.org/10.1177/0306624x12459185

[42] Helsel, D.R. and Hirsch, R.M. (2002) Statistical Methods in Water Resources. U.S. Geological Survey, Techniques of Water-Resources Investigations, Book 4, Chapter A3. https://doi.org/10.3133/twri04A3

[43] Torrence, C. and Compo, G.P. (1998) A Practical Guide to Wavelet Analysis. *Bulletin of the American Meteorological Society*, **79**, 61-78. https://doi.org/10.1175/1520-0477(1998)079<0061:apgtwa>2.0.co;2

[44] Grinsted, A., Moore, J.C., Jevrejeva, S., Grinsted, A. and Moore, J.C. (2008) Application of the Cross Wavelet Transform and Wavelet Coherence to Geophysical Time Series. *Nonlinear Processes in Geophysics*, **11**, 561-566.

[45] Viste, E. and Sorteberg, A. (2012) The Effect of Moisture Transport Variability on Ethiopian Summer Precipitation. *International Journal of Climatology*, **33**, 3106-3123. https://doi.org/10.1002/joc.3566

[46] Ding, Y., Dong, J., Meng, S., Teng, M., Yang, J. and Li, S. (2026) Long-Term Trends in Global Land Aerosol Optical Depth and Teleconnection with Sea Surface Temperature during 2000-2023. *Atmospheric Research*, **329**, Article ID: 108496. https://doi.org/10.1016/j.atmosres.2025.108496